ELSEVIER

Since January 2020 Elsevier has created a COVID-19 resource centre with free information in English and Mandarin on the novel coronavirus COVID-19. The COVID-19 resource centre is hosted on Elsevier Connect, the company's public news and information website.

Contents lists available at ScienceDirect

Antiviral Research

journal homepage: www.elsevier.com/locate/antiviral

In vitro and in vivo evaluation of the main protease inhibitor FB2001 against SARS-CoV-2

Weijuan Shang [a,1], Wenhao Dai [b,1], Cheng Yao [c,1], Ling Xu [d], Xiangming Tao [e], Haixia Su [b], Jian Li [b], Xiong Xie [b], Yechun Xu [b], Min Hu [c], Dong Xie [c], Hualiang Jiang [b,f], Leike Zhang [a,*], Hong Liu [b,**]

[a] State Key Laboratory of Virology, Wuhan Institute of Virology, Center for Biosafety Mega-Science, Chinese Academy of Sciences, Wuhan, 430071, China
[b] State Key Laboratory of Drug Research, Shanghai Institute of Materia Medica, Chinese Academy of Sciences, Shanghai, 201203, China
[c] Frontier Biotechnologies Inc., Nanjing, Jiangsu, 211122, China
[d] Shanghai University of Traditional Chinese Medicine, Shanghai, 201203, China
[e] Beijing BioVoice Technology Co., Ltd., Beijing, 100068, China
[f] Lingang Laboratory, Shanghai, 200031, China

ARTICLE INFO

ABSTRACT

FB2001 is a drug candidate that targets the main protease of SARS-CoV-2 via covalently binding to cysteine 145. In this study, we evaluated the inhibitory activities of **FB2001** against several SARS-CoV-2 variants *in vitro* and *in vivo* (in mice), and we also evaluated the histopathological analysis and immunostaining of **FB2001** on lung and brain which have been rarely reported. The results showed that **FB2001** exhibited potent antiviral efficacy against several current SARS-CoV-2 variants in Vero E6 cells, namely, B.1.1.7 (Alpha): $EC_{50} = 0.39 \pm 0.01$ μM, $EC_{90} = 0.75 \pm 0.01$ μM; B.1.351 (Beta): $EC_{50} = 0.28 \pm 0.11$ μM, $EC_{90} = 0.57 \pm 0.21$ μM; B.1.617.2 (Delta): $EC_{50} = 0.27 \pm 0.05$ μM, $EC_{90} = 0.81 \pm 0.20$ μM; B.1.1.529 (Omicron): $EC_{50} = 0.26 \pm 0.06$ μM and $EC_{50} = 0.042 \pm 0.007$ μM (in the presence of a P-glycoprotein inhibitor). **FB2001** remained potent against SARS-CoV-2 replication in the presence of high concentrations of human serum, which indicating that human serum had no significant effect on the *in vitro* inhibitory activity. Additionally, this inhibitor exhibited an additive effect against SARS-CoV-2 when combined with Remdesivir. Furthermore, **FB2001** significantly reduced the SARS-CoV-2 copy numbers and titers in the lungs and brains *in vivo*, and alleviated the pathological symptoms. In addition, **FB2001** could alleviated local bleeding, erythrocyte overflow, edema, and inflammatory cell infiltration in brain tissue, and inhibitors reducing viral titers and improving inflammation in the brain have been rarely reported. A physiologically based pharmacokinetic model was established and verified to predict the **FB2001** concentration in human lungs. When **FB2001** was administered at 200 mg twice a day for 5 days, the observed $C_{trough\ ss}$ in plasma and predicted $C_{trough\ ss}$ of lung total concentration were 0.163 and 2.5 μg/mL, which were approximately 9 and 132-fold higher than the EC_{50} of 0.019 μg/mL (0.042 μM) against Omicron variant. Taken together, our study suggests that **FB2001** is a promising therapeutic agent in COVID-19 treatment and can be combined with remdesivir to achieve improved clinical outcomes. Owing to its good safety and tolerability in healthy human (NCT05197179 and NCT04766931), **FB2001** has been approved for Phase II/III clinical trial (NCT05445934).

---

1. Introduction

The SARS-CoV-2 (severe acute respiratory syndrome coronavirus 2) and related COVID-19 (coronavirus disease 2019) have caused a large outbreak worldwide and become an increasingly serious concern to public health. The frequent emergence of SARS-CoV-2 variants with high infectivity, such as B.1.1.7 (Alpha), B.1.351 (Beta), B.1.617.2 (Delta), and B.1.1.529 (Omicron), have reduced the effectiveness of the existing vaccines (Tregoning et al., 2021). In addition, some recent studies showed that SARS-CoV-2 not only causes lung inflammation, but also causes severe brain-related abnormalities, for example, a reduction in global brain size and grey matter thickness and olfactory dysfunction. However, the deleterious impacts in the brain remains to be further investigated (de Erausquin et al., 2021; Douaud et al., 2022).

Since the beginning of the pandemic, numerous studies and clinical trials have been conducted to evaluate the effects of anti-SARS-CoV-2 therapeutics. Currently, there are two main drug groups against SARS-CoV-2: virus-directed drugs targeting proteins of the virus, and host-directed drugs targeting proteins or biological processes in the host that supports the virus (Simsek-Yavuz and Komsuoglu Celikyurt, 2021). Most of these drugs are based on repurposing existing antiviral agents, such as the nucleotide analogues Remdesivir and Galidesivir, protease inhibitors Lopinavir and Ritonavir, antimalarial drug Chloroquine, and host natural immunity booster interferon (Marei et al., 2021). However, the Solidarity clinical trial initiated by the World Health Organization has concluded that some of these treatments had little or no effect on mortality, initiation of ventilation, and duration of hospital stay in hospitalized patients. Although the disclosed data suggest that Molnupiravir (Jayk Bernal et al., 2022), Paxlovid (PF-07321332/ritonavir) (Mahase, 2021), and Ensitrelvir (S-217622) show some efficacy in clinical studies on nonhospitalized patients with mild-to-moderate COVID-19, the development of a novel specific effective treatment for COVID-19 and viral clearance of SARS-CoV-2 in the brain remains important.

Virus-encoded proteases play vital roles in the life cycle of coronaviruses. The main protease (M^{pro}, also named 3CL protease) of SARS-CoV-2 is a cysteine protease that cleaves the viral polyproteins at more than 11 sites, releasing the vital proteins required for viral replication (Thiel et al., 2003). M^{pro} is highly conserved among all coronaviruses and has no human homolog, representing an ideal antiviral target for SARS-CoV-2 and several variants (Yang et al., 2006). Some specific effective treatments that inhibit M^{pro} have entered clinical trials for treating COVID-19, including PF-07321332, and S-217622 (Aniruddhan et al., 2021; Boras et al., 2021; Owen et al., 2021; Unoh et al., 2022). Furthermore, potential M^{pro} inhibitors, such as GC373, GC376, and compounds **11r** and **13b**, have also exhibited potent anti-SARS-CoV-2 efficacy *in vitro*, and the representative main protease inhibitors were shown in Scheme S1 (Hoffman et al., 2020; Vuong et al., 2020; Zhang et al., 2020).

Previously, we reported the drug candidate **FB2001** (also named compound **11a**) with the design, synthesis, and analysis of the crystal structure of the coronavirus M^{pro}; **FB2001** exhibited potent inhibitory activity against SARS-CoV-2 *in vitro* (M^{pro}: IC$_{50}$ = 0.053 ± 0.005 μM; EC$_{50}$ = 0.53 ± 0.01 μM) (Dai et al., 2020). In this study, we further evaluated the anti-SARS-CoV-2 activity of **FB2001** *in vitro* and *in vivo* (in mice), and the histopathological analysis and immunostaining of **FB2001** in the lung and brain of mice were also evaluated. Our results suggested that **FB2001** could potently inhibit the replication of SARS-CoV-2 and several variants and reduce the copy numbers and virus titers in the lungs and brains of mice. **FB2001** could potentially alleviate the pathological symptoms in the lungs and brains. Considering the seriously brain-related abnormalities caused by SARS-CoV-2, the ability of **FB2001** to reduce viral load in the brain has important implications. In addition, according to the established physiologically based pharmacokinetic (PBPK) model, the trough concentration of **FB2001** in the human lung was predicted to be more than 132-fold higher than the EC$_{50}$ value, and the observed C$_{trough\ ss}$ in plasma was 9-fold higher than the EC$_{50}$. Therefore, **FB2001** is a promising therapeutic agent for the treatment of SARS-CoV-2 infection and has an additive antiviral effect when combined with Remdesivir.

2. Materials and methods

2.1. Antiviral testing against SARS-CoV-2 in Wuhan Institute of Virology

SARS-CoV-2 strains wild-type (2019-nCoV-WIV04), South African strain B.1.351, England strain B.1.1.7, Delta strain B.1.617.2, Omicron strain B.1.1.529 were all obtained from Microorganisms & Viruses Culture Collection Center.

2.1.1. Cell culture and treatment

African green monkey kidney Vero E6 cells (ATCC-1586) were cultured in T75 flasks and incubated at 37 °C, 5% CO$_2$. Cells were passaged at a ratio of 1:3 every 48 h. Media formula: 90% DMEM (Gibco Invitrogen), and 10% fetal bovine serum (Gibco Invitrogen).

One day prior to testing, the cell culture medium was removed and 2 mL trypsin solution was added for 1–2 min of digestion at 37 °C after the cells were rinsed once with the extra cell fluid. Medium was added, and cells were counted prior to their transfer to a 48-well plate at 50,000 cells per well.

2.1.2. Compound preparation

FB2001 (Batch #: 20190714) was dissolved in DMSO to form 40 mM stock solution. On the day of testing, the stock solution was subject to 10-fold serial dilutions with DMEM, i.e., 1 μL of stock solution was added to 9 μL of DMEM. Ten-fold dilution was performed twice to obtain 0.4 mM solution. Further diluted to obtain 20 μM solution with DMEM, followed by 3-fold serial dilution to obtain the lowest concentrations.

Positive control **PF-07321332** was dissolved in DMSO to form 40 mM stock solution. On the day of testing, the stock solution was subject to 10-fold serial dilutions with DMEM, i.e., 1 μL of stock solution was added to 9 μL of DMEM. Ten-fold dilution was performed thrice to obtain 0.04 mM solution. Further diluted to obtain 20 μM solution with DMEM, followed by 3-fold serial dilution to obtain the lowest concentrations.

The content of DMSO in the final testing concentration did not exceed 0.2%. This concentration of DMSO had no effect on the replication of SARS-CoV-2.

2.1.3. Effect of compound on viral replication

After supernatant was removed from the 48-well plate, the diluted compound was added to each well and incubated for 1 h. Cells were then inoculated with SARS-CoV-2 in biosafety level 3 (BSL-3) laboratory at multiplicity of infection (MOI) of 0.01 or 0.005, and incubated for 1 h. Thereafter, the supernatant was removed, cells were washed with PBS, and diluted compound **FB2001** with or without P-gp inhibitor CP-100356 was added. At 24 h after infection, the supernatant was collected. The viral RNA in the supernatant was extracted and used for reverse transcription. Viral RNA copy number was then determined using real-time fluorescence quantitative PCR.

2.1.4. Effect of compound on cell viability

After the supernatant has been removed from the 96-well plate, the diluted compound was added to each well, and cell viability was determined using the CCK8 assay kit after cells were incubated for 24 h.

2.1.5. Data processing and statistics analysis

Data analysis and processing were performed using GraphPad Prism 6 and Microsoft Excel. The extent of inhibition of SARS-CoV-2 by compounds at different concentrations can be calculated with the following formula:

Inhibition % = [1 − (I/Io)] × 100%Where, Inhibition % represents

the percentage of inhibition of SARS-CoV-2 replication by the compound, I and Io represent the copy numbers of SARS-CoV-2 viral RNA in the compound and control (DMSO) wells, respectively.

The EC_{50} of the compound was calculated by fitting the following equation using GraphPad Prism 6:

Y = Bottom + (Top-Bottom)/(1 + 10^(LogIC$_{50}$ - X) * HillSlope). Where, X is the Log value of the testing concentration of the sample, Y is the percentage of inhibition at the corresponding concentration, and Bottom and Top are the minimum and maximum percentage of inhibition, respectively.

2.2. Antiviral testing of FB2001 against SARS-CoV-2 in the presence of different concentrations of human serum

FB2001 (batch #: D20071301) was provided by Frontier Biotechnologies Inc. (Nanjing, Jiangsu, China). To test the antiviral effect of **FB2001** on SARS-CoV-2 in the presence of different concentrations of human serum, Vero E6 cells were inoculated with SARS-CoV-2 (2019-nCoV-WIV04) at MOI of 0.01 in a BSL-3 laboratory. The medium was removed at 1 h after incubation. Cells were washed with PBS, followed by additional 24-h incubation with different concentrations of **FB2001** (16.60, 5.55, 1.85, 0.62, and 0.21 μM) diluted in DMEM (200 μL/well) containing different concentrations of human serum (10%, 20%, 30%, 40% and 50%; H3667; Sigma-Aldrich, St. Louis, MO, USA) at 37 °C. DMSO was used as a negative control. The cell supernatant was collected at 24h after incubation. The viral RNA in the supernatant was extracted using a MiniBEST viral RNA/DNA extraction kit (#9766; Takara, Japan).

The content of DMSO in the final testing concentration did not exceed 0.2%. This concentration of DMSO had no effect on the replication of SARS-CoV-2.

2.3. Combination and interaction analysis of FB2001 and remdesivir

2.3.1. Cell culture and treatment

Vero E6 cells were cultured in T75 flasks and incubated at 37 °C, 5% CO2. Cells were passaged at a ratio of 1:3 every 48 h. Media formula: 90% DMEM (Gibco Invitrogen), and 10% fetal bovine serum (Gibco Invitrogen).

One day prior to testing, the cell culture medium was removed and the cells were rinsed once with the extracellular fluid, before 2 mL of Trypsin solution was added for 1–2 min of digestion at 37 °C. Culture medium was added and cells were counted prior to their transfer to a 96-well plate, at 20,000 cells per well.

2.3.2. Compound preparation

FB2001 (Batch #: 20190714) was dissolved in DMSO to form 40 mM stock solution. On the day of testing, the stock solution was subject to 10-fold serial dilutions with DMEM, i.e., 1 μL of stock solution was added to 9 μL of DMEM Ten-fold dilution was performed twice to obtain 0.4 mM solution. Eight-fold dilution was performed to obtain 50 μM solution, followed by DMEM gradient dilution to obtain concentrations of 5, 2.5, 1.25, 0.625, 0.3125 and 0.15625 μM. The final concentration solution of **FB2001** was mixed with different concentrations of remdesivir (GS-5734).

Remdesivir was dissolved in DMSO to form 40 mM stock solution. On the day of testing, the stock solution was subject to 10-fold serial dilutions with DMEM, i.e., 1 μL of stock solution was added to 9 μL of DMEM ten-fold dilution was performed twice to obtain 0.4 mM solution. Eight-fold dilution was performed to obtain 50 μM solution, followed by DMEM gradient dilution to obtain concentrations of 20, 10, 5, 2.5, 1.25 and 0.625 μM. The final concentration solution of remdesivir was mixed with different concentrations of **FB2001**.

The content of DMSO in the final testing concentration did not exceed 0.2%. This concentration of DMSO had no effect on the replication of SARS-CoV-2.

2.3.3. Effect of compound on viral replication by IFA

After supernatant was removed from the 96-well plate, the diluted compound (dissolved in DMEM containing different concentrations of human serum) was added to each well and incubated for 1 h. Cells were then inoculated with SARS-CoV-2 (2019-nCoV-WIV04) in biosafety level 3 (BSL-3) laboratory at multiplicity of infection (MOI) of 0.01. At 24 h after infection, the supernatant was removed, cells were fixed, and the 96-well plate was washed with PBS. After permeabilization and blocking, cells were incubated with primary and secondary antibodies, and NP content was determined using fluorescence imaging. The DMSO group was used as the control well to calculate the inhibitory rate of viral replication by the compound.

2.3.4. Data processing and statistical analysis

Data analysis and processing were performed using GraphPad Prism 6 and Microsoft Excel. The extent of inhibition of SARS-CoV-2 by compounds at different concentrations can be calculated with the following formula:

Inhibition % = [1 − (I/Io)] × 100%Where, Inhibition % represents the percentage of inhibition of SARS-CoV-2 replication by the compound, I and Io represent the fluorescence intensity of SARS-CoV-2 NP protein in the compound and control (DMSO) wells, respectively.

2.4. Antiviral testing against SARS-CoV-2 in vivo

7–8 weeks K18-hACE2 mice were purchased from Jiangsu Gem-Pharmatech Biotechnology Co., Ltd. (Jiangsu, China). All the K18-hACE2 mice were cared following the recommendations of National Institutes of Health Guidelines for the Care and Use of Experimental Animals. Viral infections were performed in biosafety level 3 (BSL-3) facility. (Ethics number: WIVA25202202).

2.4.1. Preparation of FB2001 for injection

0.9% sterile normal saline was added to one vial of **FB2001** for injection, then shaken to completely dissolve and filtered with 0.22 μm membrane to obtain **FB2001** for injection solution.

The dosage in **FB2001** for injection groups were 100 mpk and 200 mpk: According to the average body weight (23 g) of mice, the administration volume of each mouse was 0.2 mL. The concentration of **FB2001** for injection were 11.5 mg/mL and 23 mg/mL, respectively. Animals were intraperitoneally injected twice daily.

2.4.2. Preparation of vehicle negative control

0.9% sterile normal saline were used as a negative control.

Dosage: According to the average body weight (23 g) of mice, the administration volume of each mouse was 0.2 mL. Animals were intraperitoneally injected twice daily.

2.4.3. Virus challenge, drug treatment and sample collection

K18-hACE2 mice aged 7–8 weeks were transferred to BSL-3 laboratory in Wuhan Institute of Virology. Each mouse was infected with 1×10^3 PFU SARS-CoV-2 Delta variant by nasal drip, which was designated as Day 0. After 2 h of SARS-CoV-2 challenge, mice were intraperitoneally injected with **FB2001** for injection or vehicle control. A total of 21 mice were divided into 3 groups: 7 in Vehicle group (BID, intraperitoneal injection), 7 in **FB2001**-100 mpk group (BID, intraperitoneal injection) and 7 in **FB2001**-200 mpk group (BID, intraperitoneal injection). Mice were administered with **FB2001** for injection or vehicle control once daily on Day 0 and twice daily at 9-h intervals on Day 1, 2 and 3. The body weight of the mice were recorded once daily.

Four mice per group were sacrificed on Day 2, and 3 mice per group were sacrificed on Day 4. Lung and brain tissues were then removed from mice for detection of viral RNA. The right lung was ground with DMEM, part of the homogenate was taken for RNA extraction, and the rest was stored at −80 °C; The left lung was fixed with paraformaldehyde for histopathological examination.

2.4.4. Detection of viral RNA

Viral RNA from the lung and brain tissues were extracted with the kit and reverse transcribed according to the operation instruction, then the absolute viral RNA copy in the tissue was detected quantitatively by real-time quantitative PCR. The viral RNA copy was calculated by standard plasmid concentration according to the kit instruction.

2.4.5. Histological analysis

For histologic examination, mouse lungs and brains were collected directly after euthanasia and placed in 4% paraformaldehyde for >5 days after which tissues were embedded in 3.5-mm paraffin. Fixed tissue samples were used for hematoxylin-eosin (H&E) staining and immunohistochemistry (IHC) for the detection of the SARS-CoV-2 antigen (SARS-CoV-2 Nucleocapsid Protein (HL344) Rabbit mAb #26369, CST). The image information was collected using a Pannoramic MIDI system (3DHISTECH, Budapest) and FV1200 confocal microscopy (Olympus). The slices were browsed under the microscope or used CaseViewer 2.4 to view the digital slices, observed the tissue structure in detail at different magnifications, described the typical pathological changes in the slices such as inflammation, necrosis, degeneration, hyperplasia, and fibrosis, and reflected the differences between each group of mice. Representative images were selected based on the prevalent trend for a given treatment group, showing images representative of the mean pathological score.

2.5. PBPK model establishment and validation method

The physical and chemical properties were actually measured or predicted according to **FB2001** drug chemical structures, including acid-base dissociation equilibrium constant (pKa), oil-water partition coefficient (logP), log_{10} of the distribution coefficient of an ionized form of a drug molecule (logD) at a particular pH, permeability and blood/plasma concentration ratio (Rbp) and fraction unbound in plasma (Fu), see Table S4. PBPK model in SD rat and Beagle dogs was established, validated and optimized according to the concentration of **FB2001** in plasma and lung tissue concentration. The human PBPK model is established and verified according to the plasma drug concentration. After the predicted and measured values fit well, the drug concentration in human lung was predicted. The process of model building and lung concentration prediction is shown in Fig. S5A. The EC_{50} (0.042 μM = 0.019 μg/mL) of **FB2001** in Vero E6 will be used in the PBPK model simulation and estimation for effective human dose at different administration intervals. Gastroplus (version 9.8, simulations plus, USA) was used for PBPK modeling and simulation. R software (version 4.0.2) was used for drawing.

2.5.1. SD rat PBPK model and validation

The intravenous PBPK model of **FB2001** in SD rats was established using the physical and chemical properties. Then the measured plasma concentration of **FB2001** in SD rats after intravenous administration was used to optimize and validate the rat PBPK model. The optimized parameters included tissue partition coefficient (Kp) values of skin, muscle, adipose and other tissues, as shown in Figs. S5B and C. When the simulated plasma concentration of **FB2001** in SD rats was well consistent with the measured data in the rat PBPK model, the lung tissue concentration of **FB2001** in rats was predicted, optimized and validated according to the measured lung tissue drug concentration in SD rats. The key optimization parameters include permeability-surface area product for tissue (PStc), tissue partition coefficient (Kp), intracellular drug fraction unbound (Fu Int) and extracellular drug fraction unbound (Fu Ext), so that the predicted values of **FB2001** in lung tissue were consistent with the measured values. Predicted and observed PK parameters of plasma drug concentration in rats were shown in Table S5, and simulated and observed drug concentration in plasma and lung total were shown in Fig. S6A.

2.5.2. Beagle dogs PBPK model and validation

The PBPK model of **FB2001** after intravenous administration in beagle dogs was established using physical and chemical properties. Then the measured plasma concentration of **FB2001** after intravenous administration was used to optimize and validate the beagle dogs PBPK model. The optimized parameters include Kp values of skin, muscle, adipose and other tissues. When the simulated plasma concentration of **FB2001** in beagle dogs was well consistent with the measured data through intravenous administration in the beagle dog PBPK model, the lung tissue drug concentration in beagle dogs was predicted, and then optimized and validated according to the measured lung tissue concentration of **FB2001** in beagle dogs. The key parameters optimized include PSTC, KP, Fu Int and Fu Ext. The adjustment ratio of parameters was the same as that in SD rats PBPK model. The predicted values were considered reasonable if the ratio of predicted to observed data was within a predefined 2-fold range (0.5 ≤ ratio ≤2.0). Predicted and observed PK parameters of plasma drug concentration in dogs were shown in Table S5, and simulated and observed drug concentration in plasma and lung total were shown in Fig. S6B.

2.5.3. Human PBPK model and validation

The human intravenous PBPK model of **FB2001** was established using physical and chemical properties. The optimized parameters include KP values of skin, muscle, adipose and other tissues. When the simulated plasma concentration of **FB2001** in human was well consistent with the measured data in the human PBPK model, the lung tissue concentration of **FB2001** in human was predicted. The adjusted key parameters included PSTC, KP, Fu Int and Fu Ext, the adjustment ratio of the parameters was the same as that of the SD rat and beagle dogs PBPK model. Predicted lung total concentration of **FB2001** in human were shown in Table 2.

3. Results

3.1. FB2001 shows antiviral activity against several current SARS-CoV-2 variants in vitro

The antiviral effect of **FB2001** and PF-07321332 against SARS-CoV-2 and several current variants were investigated *in vitro* using by measuring viral copy number, as shown in Table 1 and Fig. S1. **FB2001**

Table 1
In vitro activity of FB2001 against SARS-CoV-2 and variants.

Virus	Compounds	EC_{50} (μM) [a]	EC_{90} (μM) [a]	CC_{50} (μM)	SI_{50} [b]
SARS-CoV-2	**FB2001**	0.42 ± 0.08	1.36 ± 1.73	274.4	653
	Chloroquine phosphate	4.17 ± 0.05	/	>100	>23.9
SARS-CoV-2 (Alpha)	**FB2001**	0.39 ± 0.01	0.75 ± 0.01	274.4	704
	PF-07321332	0.82 ± 0.02	1.54 ± 0.02	/	/
SARS-CoV-2 (Beta)	**FB2001**	0.28 ± 0.11	0.57 ± 0.21	274.4	980
	PF-07321332	0.49 ± 0.06	1.74 ± 0.26	/	/
SARS-CoV-2 (Delta)	**FB2001**	0.27 ± 0.05	0.81 ± 0.20	274.4	1016
	PF-07321332	0.78 ± 0.21	1.89 ± 0.10	/	/
SARS-CoV-2 (Omicron)	**FB2001**	0.26 ± 0.06	/	242.7	937
	PF-07321332	/	/	/	/
	FB2001+CP-100356	0.042 ± 0.007	/	142.4	3390

[a] Data from a representative experiment are shown as mean ± SD.
[b] $SI_{50} = CC_{50}/EC_{50}$.

Table 2
Predicted lung total concentration of FB2001 in human.

Dose	150 mg BID	200 mg BID	300 mg QD	400 mg QD
$C_{max, first}$ (μg/ml)	7.3	10	15	20
$C_{min, first}$ (μg/ml)	0.44	0.6	0.69	0.91
$C_{max,ss}$ (μg/ml)	9.1	12	17	22
$C_{trough,ss}$ (μg/ml)	1.8	2.5	1.7	2.2

potently inhibited the replication of SARS-CoV-2 variants (B.1.1.7 (Alpha): $EC_{50} = 0.39 \pm 0.01$ μM, $EC_{90} = 0.75 \pm 0.01$ μM; B.1.351 (Beta): $EC_{50} = 0.28 \pm 0.11$ μM, $EC_{90} = 0.57 \pm 0.21$ μM; B.1.617.2 (Delta): $EC_{50} = 0.27 \pm 0.05$ μM, $EC_{90} = 0.81 \pm 0.20$ μM; B.1.1.529 (Omicron): $EC_{50} = 0.26 \pm 0.06$ μM) in Vero E6 cells, yielding an SI_{50} of 704, 980, 1016, and 933, respectively. The inhibitory activity of **FB2001** against the SARS-CoV-2 Omicron variant was significantly increased ($EC_{50} = 0.042 \pm 0.007$ μM; $CC_{50} = 142.4$ μM) when CP-100356, an inhibitor of P-glycoprotein (P-gp), was added. Consequently, these results indicated **FB2001** might be a substrate of P-gp.

The time of addition assay also were conducted, **FB2001** (2 μM, 10 μM, 1 μM + P-gp inhibitor) were incubated with the cells for different time according to the following conditions: entry (−2 to 2 h), post entry (2–24 h) and full-time (−2 to 24h). The **FB2001** showed potent antiviral activities under all conditions, especially when administrated under two conditions: post entry and full-time (Fig. S2), and those results were in agreement with its antiviral mechanism as a main protease inhibitor. In addition, it also exhibited inhibitory effect on the process of virus entry.

Previously, crystal complexes showed that the aldehyde group of **FB2001** formed covalent bond with Cys145 of SARS-CoV-2 M^{pro} (PDB: 6LZE), and the binding modes was also proved to be reversible in this manuscript. Reversibility of M^{pro} inhibition was demonstrated upon incubation of SARS-CoV-2 M^{pro} (2 mM) with 2 μM of **FB2001**, reversible M^{pro} inhibitor (PF-07321332) or an irreversible M^{pro} inhibitor (N3) for 60 min and monitoring M^{pro} activity after 50-fold and 200-fold dilution of the incubation mixtures. The results showed that the inhibitory activity was not recovered after M^{pro} incubation with N3, and M^{pro} activity were recovered after incubation with **FB2001** and PF-07321332 which indicated that the binding model of **FB2001** with M^{pro} was reversible. In addition, compared with PF-07321332, **FB2001** was more difficult to dissociate when combined with SARS-CoV-2 M^{pro} (Fig. 1A).

We compared the amino acid sequence of M^{pro} isolates from wild-type with that from four other variants, B.1.1.7 (Alpha), B.1.351 (Beta), B.1.617.2 (Delta), and B.1.1.529 (Omicron), using multiple sequence alignment (Fig. 1B). Two mutations, K90R and P132H, were found in the M^{pro} of B.1.351 (Beta) and B.1.1.529 (Omicron), respectively, while the sequences of the M^{pro} from the other three variants wild-type, B.1.1.7 (Alpha) and B.1.617.2 (Delta) were identical. The X-ray crystal structure of the M^{pro} with **FB2001** shows that the K90R and P132H mutants were far from the ligand binding site (Fig. 1C), indicating that these mutants hardly affected the binding of **FB2001** to the M^{pro}. In other words, the K90R and P132H mutants would not affect the inhibitory activity of **FB2001** against the M^{pro} of B.1.351 (Beta) and B.1.1.529 (Omicron). Those results accord with the antiviral activity data presented in Table 1.

3.2. FB2001 inhibits SARS-CoV-2 replication in vero E6 cells in the presence of different concentrations of human serum

Because the high plasma protein binding rate of these compounds as well as binding to albumin and/or α1-acid glycoprotein in human serum may attenuate the potency of protease inhibitors (Gulati et al., 2009; Islam et al., 2016), we tested **FB2001** for anti-SARS-CoV-2 (2019-nCoV-WIV04) activity in the presence of different concentrations of human serum in Vero E6 cells (Table S1). The results showed that although the EC_{50} values of **FB2001** against SARS-CoV-2 tended to increase with the increasing concentrations of human serum (1.10 μM,

1.91 μM, 2.57 μM, 2.15 μM, and 2.40 μM in 10%, 20%, 30%, 40%, and 50% of human serum, respectively), **FB2001** remained potent in inhibiting SARS-CoV-2 replication in the presence of high concentrations of human serum. At 20–50% human serum present, the inhibitory activity of **FB2001** against SARS-CoV-2 did not change significantly, and the EC_{50} value of **FB2001** was about 2 times higher of that at 10% human serum, indicating that human serum had no significant effect on the *in vitro* inhibitory activity of **FB2001**.

3.3. Combined treatment with remdesivir and FB2001 exhibits an additive effect against SARS-CoV-2 in vitro

Remdesivir is an adenosine analogue that has shown inhibitory effects on the replication of multiple coronaviruses, including human coronaviruses, SARS-CoV, MERS-CoV, and SARS-CoV-2, by incorporating into nascent viral RNA (Brown et al., 2019; de Wit et al., 2020; Sheahan et al., 2017). Recent studies have reported that remdesivir inhibits SARS-CoV-2 replication *in vitro* with an EC_{50} of 0.77–26.9 μM (Choy et al., 2020; Kotaki et al., 2021; Pizzorno et al., 2020; Wang et al., 2020), depending on the virus strain, assay type, and calculation method. As remdesivir is the first approved treatment for COVID-19 in the United States and Europe (Lamb, 2020), and the targets of **FB2001** and remdesivir are different, the synergistic effect of combined treatment with **FB2001** and remdesivir against SARS-CoV-2 was investigated. Schloer et al. (Pizzorno et al., 2020; Schloer et al., 2021) have reported that the combination of remdesivir with the repurposed antifungal drug itraconazole or the antidepressant fluoxetine achieved a 90% reduction in infectious SARS-CoV-2 particles in Calu-3 cells with lower doses of the individual drugs. Furthermore, Kalil et al. (2021) reported that cotreatment with remdesivir and the anti-inflammatory drug baricitinib was safe and outperformed remdesivir alone in improving clinical status and reducing the time to recovery of hospitalized patients with COVID-19. These findings suggest that combining two antiviral compounds with different viral or cellular targets may achieve enhanced therapeutic effects with lower doses of the individual drugs compared with monotherapy. Thus, the synergistic effect of **FB2001** and remdesivir was explored. The inhibitory activity of the combination of **FB2001** and remdesivir at different concentrations against SARS-CoV-2 was determined *in vitro*, and the detailed study results are shown in Table S2 and Fig. 2. The inhibition rate of the combination of **FB2001** and remdesivir was determined using the Synergyfinder package (Ianevski et al., 2020). The Zero interaction potency (ZIP) model was used to calculate the synergy score of **FB2001** combined with remdesivir, which was 6.947 (Fig. 2). It was found that the inhibitory activity against SARS-CoV-2 increased after administration of the combination of both compounds, and the combined effect was mainly an additive effect rather than a synergistic effect.

3.4. In vivo inhibitory activity of FB2001 in K18-hACE2 mice model of SARS-CoV-2 delta variant infection

Next, we investigated the efficacy of **FB2001** in K18-hACE2 mice challenged with SARS-CoV-2 (Delta variant). After 2 h of challenge, the mice were injected intraperitoneally, once daily on day 0 and twice daily on day 1, 2 and 3, with **FB2001** or vehicle control for 4 consecutive days (Fig. 3A). Mice were euthanized and dissected on day 2 and 4. Lung and brain tissues were removed for the detection of viral RNA and viral titer, and histopathological analysis and immunostaining of lungs and brains were also evaluated.

The weights of mice on day 0 were used as control. There is no significant change in the body weight of the mice in control group and treatment groups (**FB2001**-100 mpk (mg/kg) group and **FB2001**-200 mpk group). It was also discovered that the virus titers of the **FB2001** groups in the lung presented a dose-dependent efficacy, and the virus titers of the **FB2001**-200 mpk group showed a 3.57 $\log_{10}$ PFU/g reduction on day 2, which was then decreased to below the detection
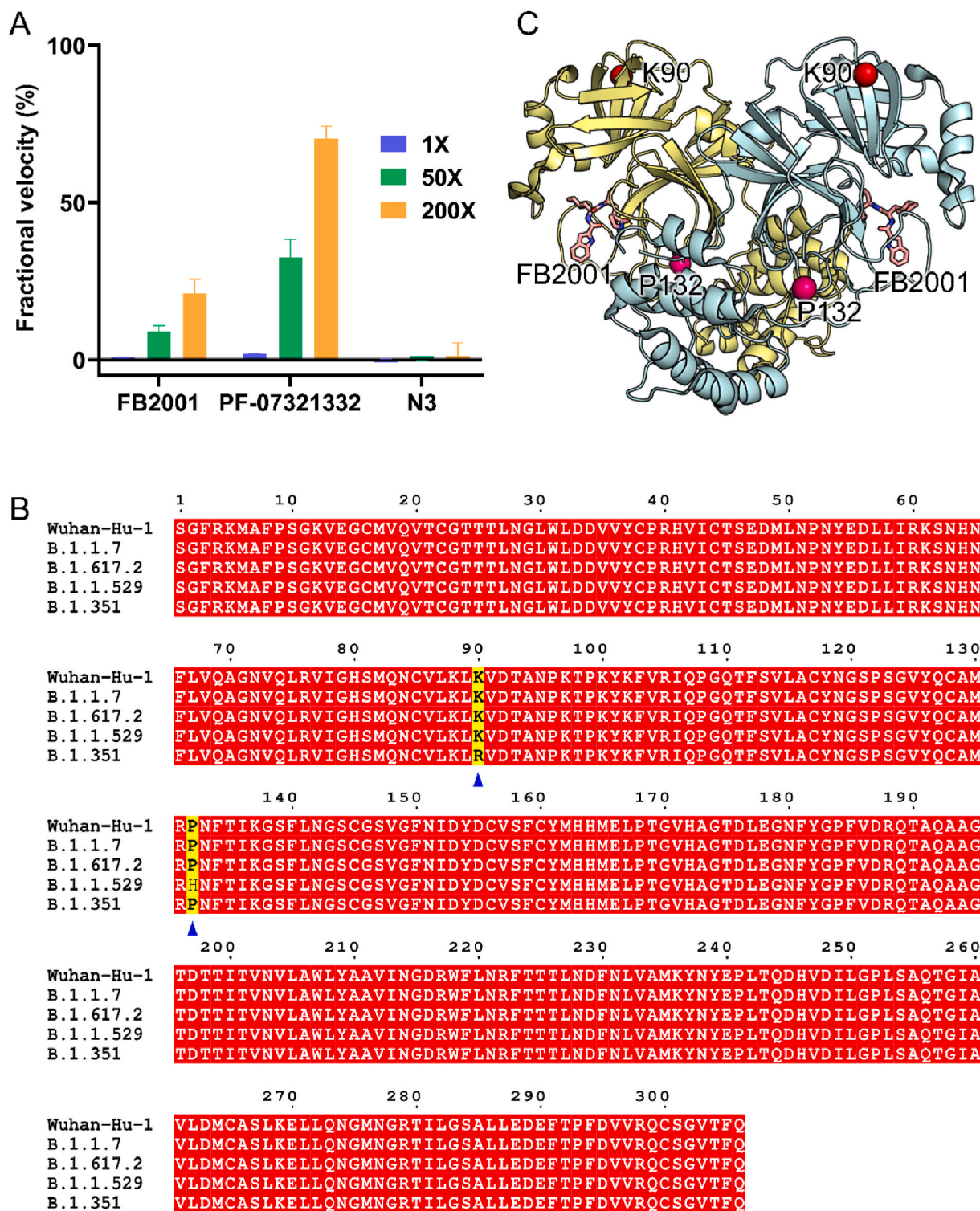
Fig. 1. Comparing the M^{pro} of SARS-CoV-2 with four SARS-CoV-2 variants of concern (VOCs). (A) **FB2001** is a reversible inhibitor of SARS-CoV-2 M^{pro} as demonstrated by recovery of enzymatic activity. (**B**) Sequence alignment of M^{pro} in SARS-CoV-2 and several variants, wild-type, B.1.1.7 (Alpha), B.1.351 (Beta), B.1.617.2 (Delta), and B.1.1.529 (Omicron). (**C**) An X-ray crystal structure of SARS-CoV-2 M^{pro} in complex with **FB2001** (PDB code: 6LZE). Compound **FB2001** is shown as pink sticks. K90, P132 and **FB2001** are indicated by red spheres, pink spheres and pink sticks, respectively.

limit at day 4 (Fig. 3B and C). And the viral titers of the **FB2001**-200 mpk group were reduced to below the detection limit on day 4 in the brain (Fig. 3D). Compared with the vehicle group, the lung viral loads in the **FB2001**-100 mpk group and **FB2001**-200 mpk group were reduced by 1.02 and 1.60 log$_{10}$ copies/g on day 2, respectively, and 0.67 and 1.14 log$_{10}$ copies/g on day 4, respectively (Figs. S3A and S3B). In addition,

compared with the vehicle group, the brain viral loads were significantly reduced by 2.37 and 5.26 log$_{10}$ copies/g in the **FB2001**-100 mpk group and **FB2001**-200 mpk group on day 4, respectively (Fig. S3C, **S3D**). The detailed data are summarized in Table S3. The antiviral activity of **FB2001** against the SARS-CoV-2 Delta variant was dose-dependent, and both 100 mpk **FB2001** and 200 mpk **FB2001** could significantly reduce

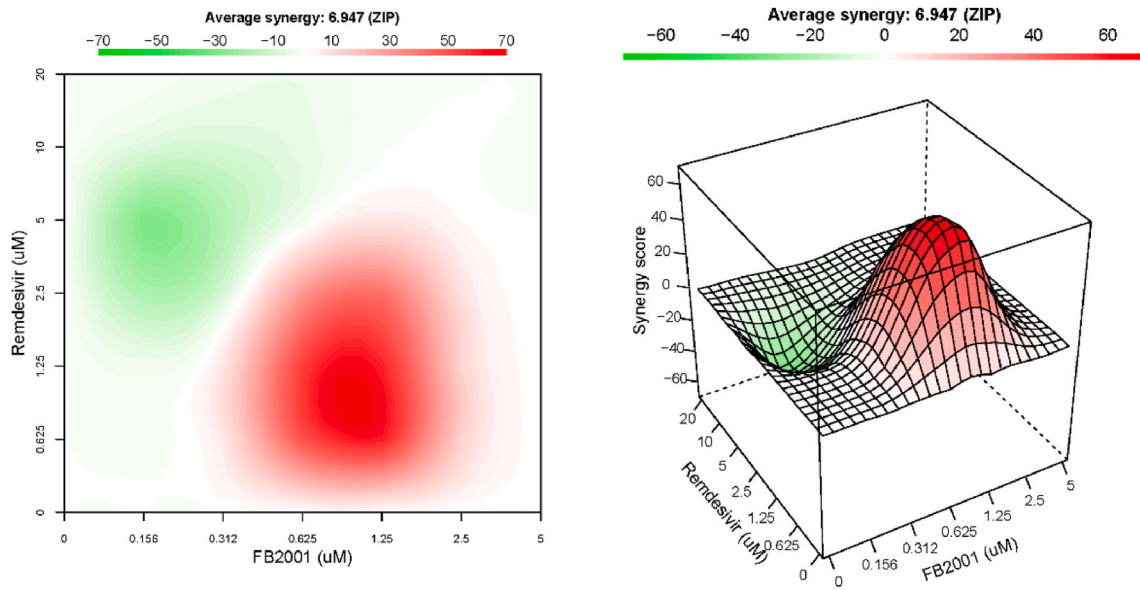**Fig. 2. Synergistic analysis of FB2001 combined with remdesivir.** Where $-10 <$ synergy score <10 indicates an additive effect, synergy score < -10 indicates an antagonistic effect, and synergy score >10 indicates a synergistic effect.
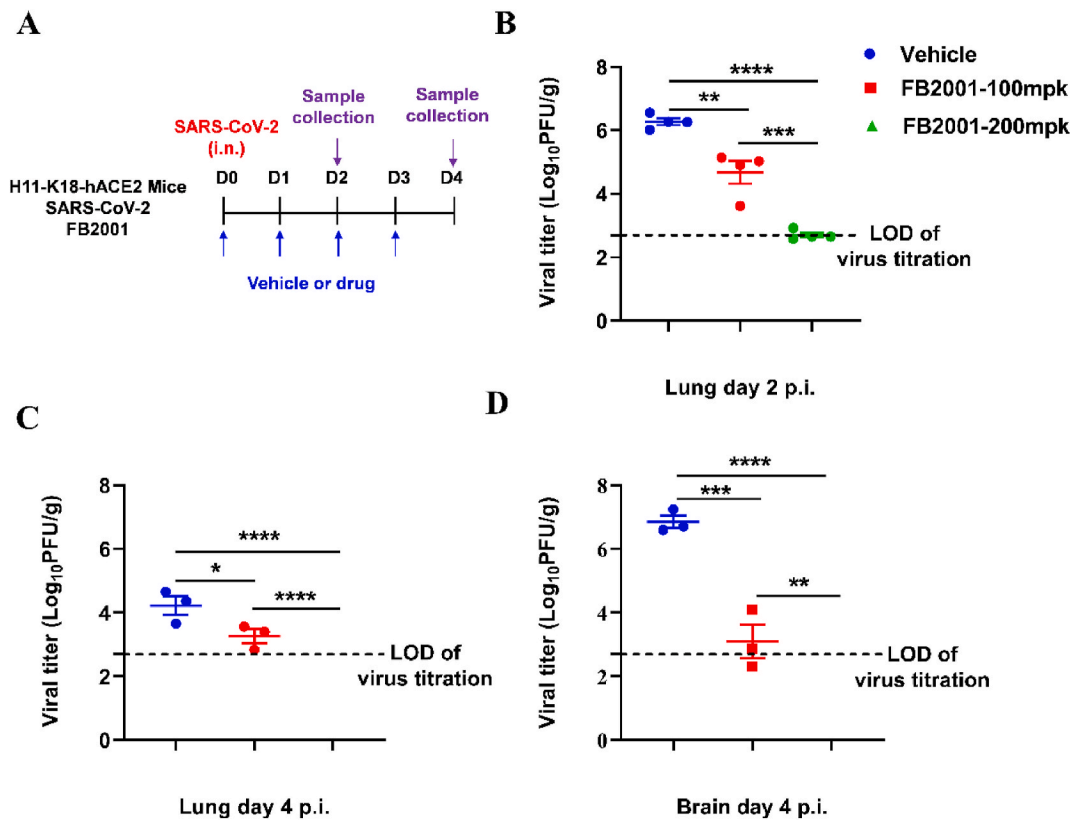

Fig. 3. *In vivo* efficacy of FB2001 in K18-hACE2 mice infected with SARS-CoV-2 delta variant. The transgenic K18-hACE2 mice were divided into 3 groups: Vehicle control group, FB2001-100 mg/kg (100 mpk) group and FB2001-200 mg/kg (200 mpk) group. 7 mice per group. Transgenic mice in treatment group were challenged with SARS-CoV-2 delta variant by nasal drip. (**A**) Experiment flow diagram. (**B, C**) Viral titer in lung on Day 2 and 4 after SARS-CoV-2 challenge (Log$_{10}$ PFU/g). Dotted line represents the limit of detection of virus titration. (**D**) Viral titer in brain on Day 4 after SARS-CoV-2 challenge (Log$_{10}$ PFU/g). Dotted line represents the limit of detection of virus titration.

viral load in mouse lung and brain. Considering the serious brain-related abnormalities caused by SARS-CoV-2, that **FB2001** could reduce viral load in the brain has important implications.

3.5. Histopathology and immunohistochemical results of FB2001 in K18-hACE2 mice model of SARS-CoV-2 delta variant infection

Representative images from hematoxylin and eosin stains of tissues

of infected K18-hACE2 transgenic mice showed that **FB2001** treatment significantly improved the histopathology in both the lung and brain compared with that of the control group. The lungs of the mice in the control group showed moderate incremental lymphoplasmacytic, histiocytic perivascular infiltrates and alveolar septal thickening observed at day 2 and day 4 (black arrows, Fig. 4B and H). In contrast, the lungs in the **FB2001**-100 mpk group showed mild interstitial inflammatory cell infiltration (red arrows, Fig. 4D and J), and decreased inflammation and normal alveolar spaces were observed in lungs of the **FB2001**-200 mpk group (Fig. 4F, L). Immunohistochemistry staining targeting viral NP demonstrated that **FB2001** suppressed viral titer in mice lungs in a dose-dependent manner (Fig. S4A–L), and the virus was almost cleared at day 4 in both the **FB2001**-100 mpk and **FB2001**-200 mpk groups.

Histopathological analysis and immunostaining of brains from the SARS-CoV-2 Delta variant–infected K18-hACE2 transgenic mice showed that **FB2001** limited cellular infiltration (Fig. 4M–R) and protected brain tissue from damage caused by virus replication at day 4 (Fig. S4M–R). Neuronal cells were neatly arranged and tightly arranged, some neurons were degenerated, the cell body was solidified and deeply stained, and the nissl body disappeared in the control group (black arrow, Fig. 4N). The arrangement of neuronal cells in the cerebral cortex was more disordered, some neurons were denatured, and the staining was deepened in the **FB2001**-100 mpk group (black arrow, Fig. 4P). Neuronal cells were neatly arranged and abundant, and the nissl body was normal in the **FB2001**-200 mpk group (Fig. 4R). Immunohistochemistry staining targeting viral NP demonstrated that **FB2001** suppressed viral titer in mice brains in a dose-dependent manner, and the virus was nearly cleared at day 4 in both the **FB2001**-100 mpk and **FB2001**-200 mpk groups (Fig. S4).

3.6. Projected effective dose

SARS-CoV-2 is rarely detected in blood, and the main viral target organs are the respiratory tract and lungs. We established a PBPK model to predict total lung drug concentration (Figs. S5 and S6 and Table S4). The model was validated using plasma and lung **FB2001** concentration

in rat and dogs (Table S5). For 200 mg BID **FB2001** administered for 5 consecutive days in human, the plasma trough concentration ($C_{trough\ ss}$) of **FB2001** was observed to be 0.163 µg/mL, and the total lung trough concentration ($C_{trough,\ SS}$) of **FB2001** was predicted to be 2.5 µg/mL (Table 2). In a Vero E6 cell–based *in vitro* antiviral assay, in the presence of the P-gp efflux inhibitor, the EC_{50} of **FB2001** against SARS-CoV-2 Omicron (B1.1.529) variant was 0.019 µg/mL. Thus, the above $C_{trough\ ss}$ of **FB2001** in plasma and lung were 9 and 132-fold higher than the EC_{50} values, respectively. The molecule also showed similar antiviral activity against the SARS-CoV-2 Delta variant.

Based on this analysis, dosage of 200 mg **FB2001** BID may offer a highest trough lung concentration, which could become an effective dosage in future clinical studies.

4. Discussion

In the past two decades, three coronaviruses (SARS-CoV, MERS-CoV, and SARS-CoV-2) have seriously affected human life and social stability. The COVID-19 pandemic, especially, has caused the death of millions of lives worldwide. Furthermore, multiple SARS-CoV-2 variants are emerging and reducing the effectiveness of vaccines. SARS-CoV-2 not only causes pneumonia, but recent studies have shown that it can also cause brain-related abnormalities, for example, the reduction in global brain size and grey matter thickness; thus, the development of effective drugs remains of paramount importance. In this study, we found **FB2001** showed potent inhibitory activity against SARS-CoV-2 and its variants. **FB2001** used in combination with remdesivir exhibited an additive effect against SARS-CoV-2 *in vitro*. In addition, **FB2001** decreased the viral loads and viral titers of the lung and brain in a SARS-CoV-2 Delta variant model, and **FB2001** treatment significantly improved the histopathology in both the lung and brain. Notably, **FB2001** significantly reduced viral titers and alleviated brain damage in the brain of mice, which were rarely reported previously. SARS-CoV-2 is mainly detected in the respiratory tract and lungs, hence, a PBPK model was established to predict total lung drug concentration. For 200 mg BID **FB2001** administered for 5 consecutive days, the total lung $C_{trough\ ss}$ of
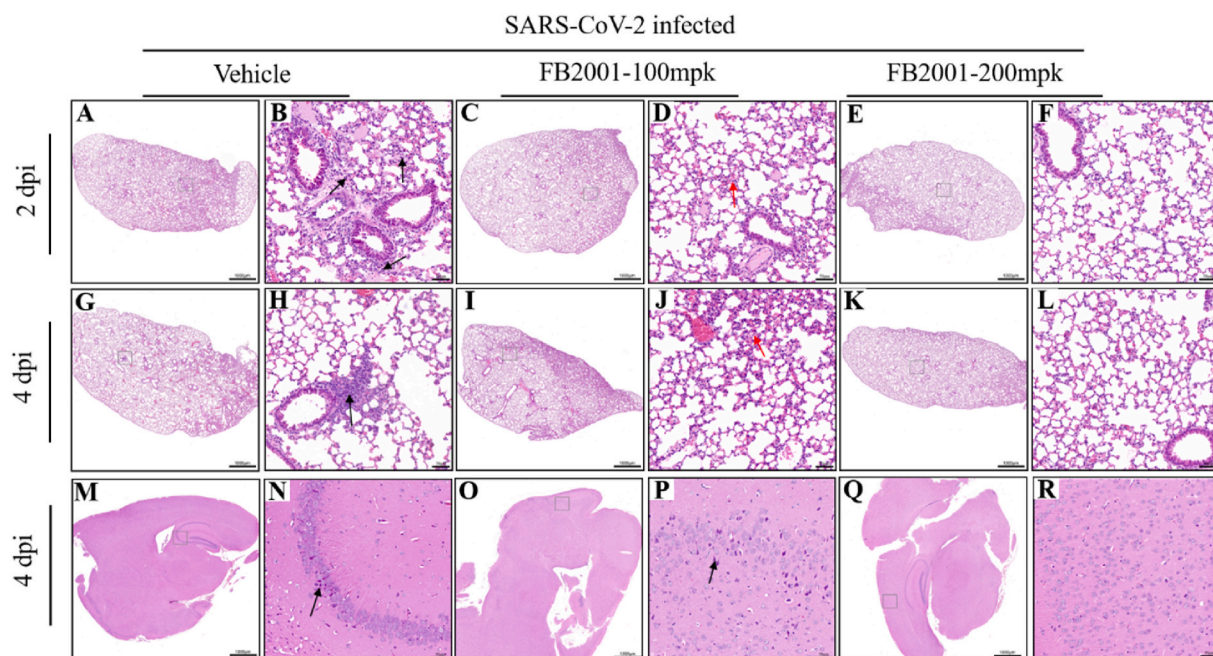

Fig. 4. FB2001 protects lung and brain tissue from damage caused by SARS-CoV-2 delta variant. (A-L) Representative H&E images of lung histopathology from vehicle-and **FB2001**-treated K18-hACE2 mice at 2 dpi and 4 dpi. Vehicle group (**A-B**: day 2 and **G-H**: day 4); **FB2001** group treated with 100 mpk drug (**C-D**: day 2 and **I-J**: day 4); **FB2001** group treated with 200 mpk drug (**E-F**: day 2 and **K-L**: day 4). (**M-R**) Representative H&E images of brain histopathology from vehicle-and **FB2001**-treated K18-hACE2 mice at day 4. Vehicle group (**M-N**); **FB2001** group treated with 100 mpk drug (**O-P**); **FB2001** group treated with 200 mpk drug (**Q-R**). Scale bar: A, C, E, G, I, K, M, O, Q = 1000 µm; B, D, F, H, J, L, N, P, R = 50 µm.

FB2001 was predicted to be 132-fold higher than the EC_{50} values, and the observed plasma $C_{trough\ ss}$ of **FB2001** was observed to be 9-fold higher than the EC_{50} values. Based on the PBPK results, 200 mg **FB2001** BID could become an effective dosage in future clinical studies.

In summary, **FB2001** exhibited broad-spectrum activity against several coronaviruses, and also showed additive antiviral effect when combined with remdesivir. In addition, **FB2001** could significantly reduce the viral loads and titers in the lungs and brain of mice infected with SARS-CoV-2. Moreover, **FB2001** has been approved for Phase II/III clinical trials, and presents a potentially good treatment for COVID-19.

Funding

Author contributions

L.K.Z., W.H.D., C.Y., W.J.S., D.X., H.L.J., and H.L., planned and designed experiments. W.H.D., J.L., X.X., synthesized the compound. H. X.S., and Y.C.X., compared the amino acid sequence. L.K.Z., W.J.S., carried out the experiments *in vitro* and *in vivo*. L.X., and X.M.T., carried out the PBPK. L.K.Z., W.H.D., C.Y., W.J.S. J.L., M.H., D.X., H.L.J., and H. L., analyzed the data. L.K.Z., W.H.D., C.Y., D.X., H.L.J., and H.L., prepared the manuscript.

Declaration of competing interest

The author(s) declared no potential conflicts of interest with respect to the research.

Data availability

Data will be made available on request.

Acknowledgements

Appendix A. Supplementary data

Supplementary data to this article can be found online at https://doi. org/10.1016/j.antiviral.2022.105450.

References

Anirudhan, V., Lee, H., Cheng, H., Cooper, L., Rong, L., 2021. Targeting SARS-CoV-2 viral proteases as a therapeutic strategy to treat COVID-19. J. Med. Virol. 93, 2722–2734. https://doi.org/10.1002/jmv.26814.

Boras, B., Jones, R.M., Anson, B.J., Arenson, D., Aschenbrenner, L., Bakowski, M.A., Beutler, N., Binder, J., Chen, E., Eng, H., et al., 2021. Preclinical characterization of an intravenous coronavirus 3CL protease inhibitor for the potential treatment of COVID19. Nat. Commun. 12, 6055. https://doi.org/10.1038/s41467-021-26239-2.

Brown, A.J., Won, J.J., Graham, R.L., Dinnon 3rd, K.H., Sims, A.C., Feng, J.Y., Cihlar, T., Denison, M.R., Baric, R.S., Sheahan, T.P., 2019. Broad spectrum antiviral remdesivir inhibits human endemic and zoonotic deltacoronaviruses with a highly divergent RNA dependent RNA polymerase. Antivir. Res. 169, 104541 https://doi.org/ 10.1016/j.antiviral.2019.104541.

Choy, K.T., Wong, A.Y., Kaewpreedee, P., Sia, S.F., Chen, D., Hui, K.P.Y., Chu, D.K.W., Chan, M.C.W., Cheung, P.P., Huang, X., et al., 2020. Remdesivir, lopinavir, emetine, and homoharringtonine inhibit SARS-CoV-2 replication in vitro. Antivir. Res. 178, 104786 https://doi.org/10.1016/j.antiviral.2020.104786.

Dai, W., Zhang, B., Jiang, X.M., Su, H., Li, J., Zhao, Y., Xie, X., Jin, Z., Peng, J., Liu, F., et al., 2020. Structure-based design of antiviral drug candidates targeting the SARS-CoV-2 main protease. Science 368, 1331–1335. https://doi.org/10.1126/science. abb4489.

de Erausquin, G.A., Snyder, H., Carrillo, M., Hosseini, A.A., Brugha, T.S., Seshadri, S., Consortium, C.S.-C.-., 2021. The chronic neuropsychiatric sequelae of COVID-19: the need for a prospective study of viral impact on brain functioning. Alzheimers Dement 17, 1056–1065. https://doi.org/10.1002/alz.12255.

de Wit, E., Feldmann, F., Cronin, J., Jordan, R., Okumura, A., Thomas, T., Scott, D., Cihlar, T., Feldmann, H., 2020. Prophylactic and therapeutic remdesivir (GS-5734) treatment in the rhesus macaque model of MERS-CoV infection. Proc. Natl. Acad. Sci. U.S.A. 117, 6771–6776. https://doi.org/10.1073/pnas.1922083117.

Douaud, G., Lee, S., Alfaro-Almagro, F., Arthofer, C., Wang, C., McCarthy, P., Lange, F., Andersson, J.L.R., Griffanti, L., Duff, E., et al., 2022. SARS-CoV-2 is associated with changes in brain structure in UK Biobank. Nature 604, 697–707. https://doi.org/ 10.1038/s41586-022-04569-5.

Gulati, A., Boudinot, F.D., Gerk, P.M., 2009. Binding of lopinavir to human alpha1-acid glycoprotein and serum albumin. Drug Metab. Dispos. 37, 1572–1575. https://doi. org/10.1124/dmd.109.026708.

Hoffman, R.L., Kania, R.S., Brothers, M.A., Davies, J.F., Ferre, R.A., Gajiwala, K.S., He, M., Hogan, R.J., Kozminski, K., Li, L.Y., et al., 2020. Discovery of ketone-based covalent inhibitors of coronavirus 3CL proteases for the potential therapeutic treatment of COVID-19. J. Med. Chem. 63, 12725–12747. https://doi.org/10.1021/ acs.jmedchem.0c01063.

Ianevski, A., Giri, A.K., Aittokallio, T., 2020. SynergyFinder 2.0: visual analytics of multi-drug combination synergies. Nucleic Acids Res. 48, W488–W493. https://doi.org/ 10.1093/nar/gkaa216.

Islam, M.M., Gurung, A.B., Bhattacharjee, A., Aguan, K., Mitra, S., 2016. Human serum albumin reduces the potency of acetylcholinesterase inhibitor based drugs for Alzheimer's disease. Chem. Biol. Interact. 249, 1–9. https://doi.org/10.1016/j. cbi.2016.02.012.

Jayk Bernal, A., Gomes da Silva, M.M., Musungaie, D.B., Kovalchuk, E., Gonzalez, A., Delos Reyes, V., Martin-Quiros, A., Caraco, Y., Williams-Diaz, A., Brown, M.L., et al., 2022. Molnupiravir for oral treatment of covid-19 in nonhospitalized patients. N. Engl. J. Med. 386, 509–520. https://doi.org/10.1056/NEJMoa2116044.

Kalil, A.C., Patterson, T.F., Mehta, A.K., Tomashek, K.M., Wolfe, C.R., Ghazaryan, V., Marconi, V.C., Ruiz-Palacios, G.M., Hsieh, L., Kline, S., et al., 2021. Baricitinib plus remdesivir for hospitalized adults with covid-19. N. Engl. J. Med. 384, 795–807. https://doi.org/10.1056/NEJMoa2031994.

Kotaki, T., Xie, X., Shi, P.Y., Kameoka, M., 2021. A PCR amplicon-based SARS-CoV-2 replicon for antiviral evaluation. Sci. Rep. 11, 2229. https://doi.org/10.1038/ s41598-021-82055-0.

Lamb, Y.N., 2020. Remdesivir: first approval. Drugs 80, 1355–1363. https://doi.org/ 10.1007/s40265-020-01378-w.

Mahase, E., 2021. Covid-19: pfizer's paxlovid is 89% effective in patients at risk of serious illness, company reports. BMJ 375, n2713. https://doi.org/10.1136/bmj. n2713.

Marei, H.E., Althani, A., Afifi, N., Pozzoli, G., Caceci, T., Angelini, F., Cenciarelli, C., 2021. Pandemic COVID-19 caused by SARS-CoV-2: genetic structure, vaccination, and therapeutic approaches. Mol. Biol. Rep. 48, 6513–6524. https://doi.org/ 10.1007/s11033-021-06630-4.

Owen, D.R., Allerton, C.M.N., Anderson, A.S., Aschenbrenner, L., Avery, M., Berritt, S., Boras, B., Cardin, R.D., Carlo, A., Coffman, K.J., et al., 2021. An oral SARS-CoV-2 M (pro) inhibitor clinical candidate for the treatment of COVID-19. Science 374, 1586–1593. https://doi.org/10.1126/science.abl4784.

Pizzorno, A., Padey, B., Dubois, J., Julien, T., Traversier, A., Duliere, V., Brun, P., Lina, B., Rosa-Calatrava, M., Terrier, O., 2020. In vitro evaluation of antiviral activity of single and combined repurposable drugs against SARS-CoV-2. Antivir. Res. 181, 104878 https://doi.org/10.1016/j.antiviral.2020.104878.

Schloer, S., Brunotte, L., Mecate-Zambrano, A., Zheng, S., Tang, J., Ludwig, S., Rescher, U., 2021. Drug synergy of combinatory treatment with remdesivir and the repurposed drugs fluoxetine and itraconazole effectively impairs SARS-CoV-2 infection in vitro. Br. J. Pharmacol. 178, 2339–2350. https://doi.org/10.1111/ bph.15418.

Sheahan, T.P., Sims, A.C., Graham, R.L., Menachery, V.D., Gralinski, L.E., Case, J.B., Leist, S.R., Pyrc, K., Feng, J.Y., Trantcheva, I., et al., 2017. Broad-spectrum antiviral GS-5734 inhibits both epidemic and zoonotic coronaviruses. Sci. Transl. Med. 9 https://doi.org/10.1126/scitranslmed.aal3653.

Simsek-Yavuz, S., Komsuoglu Celikyurt, F.I., 2021. An update of anti-viral treatment of COVID-19. Turk. J. Med. Sci. 51, 3372–3390. https://doi.org/10.3906/sag-2106-250.

Thiel, V., Ivanov, K.A., Putics, A., Hertzig, T., Schelle, B., Bayer, S., Weissbrich, B., Snijder, E.J., Rabenau, H., Doerr, H.W., et al., 2003. Mechanisms and enzymes involved in SARS coronavirus genome expression. J. Gen. Virol. 84, 2305–2315. https://doi.org/10.1099/vir.0.19424-0.

Tregoning, J.S., Flight, K.E., Higham, S.L., Wang, Z., Pierce, B.F., 2021. Progress of the COVID-19 vaccine effort: viruses, vaccines and variants versus efficacy, effectiveness and escape. Nat. Rev. Immunol. 21, 626–636. https://doi.org/10.1038/s41577-021-00592-1.

Unoh, Y., Uehara, S., Nakahara, K., Nobori, H., Yamatsu, Y., Yamamoto, S., Maruyama, Y., Taoda, Y., Kasamatsu, K., Suto, T., et al., 2022. Discovery of S-217622, a noncovalent oral SARS-CoV-2 3CL protease inhibitor clinical candidate for

treating COVID-19. J. Med. Chem. 65, 6499–6512. https://doi.org/10.1021/acs.jmedchem.2c00117.

Vuong, W., Khan, M.B., Fischer, C., Arutyunova, E., Lamer, T., Shields, J., Saffran, H.A., McKay, R.T., van Belkum, M.J., Joyce, M.A., et al., 2020. Feline coronavirus drug inhibits the main protease of SARS-CoV-2 and blocks virus replication. Nat. Commun. 11, 4282. https://doi.org/10.1038/s41467-020-18096-2.

Wang, M., Cao, R., Zhang, L., Yang, X., Liu, J., Xu, M., Shi, Z., Hu, Z., Zhong, W., Xiao, G., 2020. Remdesivir and chloroquine effectively inhibit the recently emerged novel coronavirus (2019-nCoV) in vitro. Cell Res. 30, 269–271. https://doi.org/10.1038/s41422-020-0282-0.

Yang, H., Bartlam, M., Rao, Z., 2006. Drug design targeting the main protease, the Achilles' heel of coronaviruses. Curr. Pharmaceut. Des. 12, 4573–4590. https://doi.org/10.2174/138161206779010369.

Zhang, L., Lin, D., Sun, X., Curth, U., Drosten, C., Sauerhering, L., Becker, S., Rox, K., Hilgenfeld, R., 2020. Crystal structure of SARS-CoV-2 main protease provides a basis for design of improved alpha-ketoamide inhibitors. Science 368, 409–412. https://doi.org/10.1126/science.abb3405.